Creation of Single-Photon Emitters in WSe₂ Monolayers Using Nanometer-Sized Gold Tips

Lintao Peng,¹ Henry Chan,¹ Priscilla Choo,^{2,3} Teri W. Odom,^{2,3} Subramanian K. R. S. Sankaranarayanan,^{1,4} Xuedan Ma^{1*}

¹Center for Nanoscale Materials, Argonne National Laboratory, Lemont, Illinois 60439, United States

²Department of Chemistry, Northwestern University, Evanston, Illinois 60208, United States

³Department of Materials Science and Engineering, Northwestern University, Evanston, Illinois 60208, United States

⁴Department of Mechanical and Industrial Engineering, University of Illinois, Chicago, IL 60607

Abstract

Due to their tunable bandgaps and strong spin-valley locking, transition metal dichalcogenides constitute a unique platform for hosting single-photon emitters. Here, we present a versatile approach for creating bright single-photon emitters in WSe₂ monolayers by the deposition of gold nanostars. Our molecular dynamics simulations reveal that the formation of the quantum emitters is caused by the highly localized strain fields created by the sharp tips of the gold nanostars. The surface plasmon modes supported by the gold nanostars can change the local electromagnetic fields in the vicinity of the quantum emitters, leading to their enhanced emission intensities. Moreover, by correlating the emission energies and intensities of the quantum emitters, we are able to associate them with two types of strain fields, and derive the existence of a low-lying dark state in their electronic structures. Our findings are highly relevant for the development and understanding of single-photon emitters in transition metal dichalcogenide materials.

Keywords: WSe₂ monolayers, quantum defects, strain, single photon source, dark state, surface plasmon

Quantum emitters in transition metal dichalcogenide (TMD) monolayers have recently been discovered as efficient single photon sources.¹⁻⁷ Coupled with the atomic layer thickness and distinct mechanical and optoelectronic properties of TMDs, quantum emitters in TMDs can be seamlessly integrated with photonic structures⁸⁻¹⁰ and have their bandgaps modulated using external electric^{1,11} or strain fields¹² for post-creation emission tuning. Moreover, due to the strong spin-valley coupling in TMDs, the quantum emitters may well inherit the valley physics of the host bulk TMDs,^{13,14} thus opening the possibility for the direct integration of valley degree of freedom into single photon emission.

Although the detailed microscopic origin of the quantum emitters in TMDs is still under debate, ¹⁵⁻¹⁷ it is commonly observed that localized strains are associated with the physical origins of the quantum emitters. It has therefore been suggested that strain gradient helps funnel excitons into localized point defects and lead to single photon emission. ¹⁸ To date, local strains have been engineered to deterministically create quantum emitters in TMDs. Transfer of monolayer TMD flakes onto lithographically patterned nanopillars or similar structures can create quantum emitters at highly strained locations, e.g. at the top of the nanopillars, ¹⁸⁻²⁰ thus enabling parallel creation of quantum defect arrays in relatively large scale areas. The spatial positioning accuracy of the quantum emitters in these systems is typically at the hundred nanometer scale. Alternatively, controlled ion bombardment of monolayer MoS₂ has been demonstrated to create quantum emitters that are capable of single photon emission. ²¹ With this approach, the positioning accuracy of the quantum emitters can potentially be pushed to the nanometer scales, which may enable the

study of coupled quantum emitters and interacting excitons.²¹ Compared to large scale strain engineering, however, spatially-resolved ion irradiation of TMDs is likely to make more impacts in selective creation of quantum emitters.

Here, we present an alternative approach to create quantum emitters in WSe₂ monolayers. Specifically, we utilize the nanometer-sized sharp tips of gold nanostars (AuNS) to create local strains in WSe₂ monolayers (Fig. 1a) and observe single photon emission from the created quantum emitters. Due to the coupling between the quantum emitters created at the tip ends and the AuNS surface plasmons, photoluminescence (PL) enhancement and lifetime reduction could be observed. Moreover, by correlating the emission energies and PL intensities of the quantum emitters, we are able to associate them with the types of strains they experience and derive the existence of an intrinsic low-lying dark state in the quantum emitters. Our work may not only shed light on the intrinsic electronic fine structures of the quantum emitters in TMDs, but also presents an alternative approach that can be combined with nanopositioning techniques²²⁻²⁵ and an extensive category of synthetic colloidal nanoparticles^{26, 27} for creating single-photon emitters with hybrid properties inherited from the TMD materials and colloidal nanoparticles.

AuNS used in this work were synthesized following a previously reported method (see Supporting Information S1 for details). Representative TEM images of the AuNS are shown in Fig. 1b, with majority of them possessing five short branches and one long branch. The core sizes of the AuNS are about 10 - 20 nm in diameter and the branch lengths vary from 20 to 50 nm. The branch tips typically taper down to 2 - 3 nm in thickness. This AuNS structure gives rise to a broad resonance peak centered at around 1.56 eV (Fig. 1c). The AuNS are dispersed onto monolayer WSe₂ flakes that have been mechanically exfoliated onto silicon substrates. By doing so, the AuNS simultaneously serve two purposes – their sharp tips can potentially induce local strains with

extremely small spatial footprints; the surface plasmon hotspots at the tip ends can couple to the emission from the WSe₂ monolayers. Fig. 1d shows the simulated local electric field enhancement factor distribution ($|\mathbf{E}|^2/|\mathbf{E}_0|^2$) in the vicinity of a AuNS at the energy of 1.72 eV using the finite-difference time-domain method. The field enhancement factor near the sharp tips can reach up to a few thousands, consistent with previous plasmon hybridization analysis carried out on similar

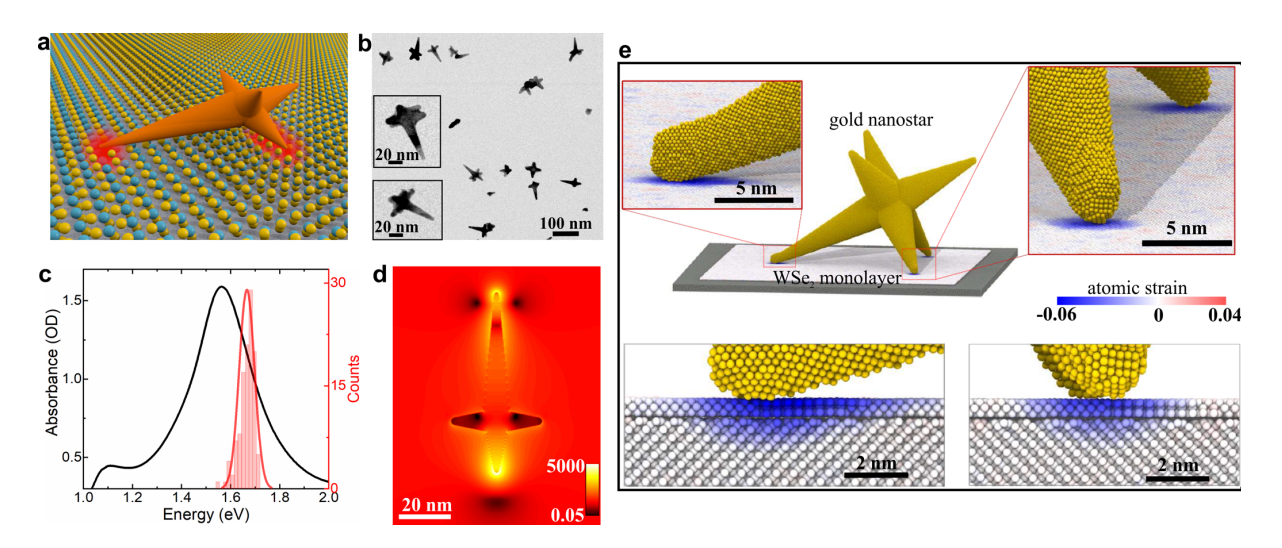


Figure 1. (a) Schematics of AuNS deposited on a monolayer WSe₂ flake. (b) Representative TEM images of the AuNS. (c) Absorbance spectrum of the AuNS solutions (black) and histogram of the quantum emitter spectral peaks (red). (d) Local electric field enhancement factor ($|\mathbf{E}|^2/|\mathbf{E}_0|^2$) in the vicinity of a AuNS at the energy of 1.72 eV simulated using the finite-difference time-domain method. The incident light is polarized along the long branch of the AuNS. (e) Large-scale molecular dynamics simulation of the strain field in a WSe₂ monolayer induced by a AuNS. Top panel: the atomistic model consisting of a 100 nm x 100 nm WSe₂ monolayer on a 3 nm thick silicon substrate and the AuNS on top. The insets are close-up views of the contact areas between the WSe₂ monolayer and the long and short arms of the AuNS. Atoms in the WSe₂ monolayer are colored based on their volumetric strain values. Bottom panel: cross-section views of the areas shown in the top panel insets, showing the penetration depths of the deformation field created by the AuNS.

structures.²⁹ This immense field enhancement can cause large modulations to the emission properties of the underlying WSe₂ monolayers.

To elucidate the strain field created by the AuNS, we perform all-atom molecular dynamics simulations to investigate the mechanical deformation of a WSe₂ monolayer upon the deposition of AuNS. The simulated system consists a WSe₂ monolayer (~ 100 nm x 100 nm x 0.3 nm, ~ 300,000 atoms) on a silicon substrate (~ 115 nm x 115 nm x 3 nm, 2 million atoms) and a AuNS positioned above the monolayer (Fig. 1e). The AuNS is modeled based on the average shape and size of those observed in TEM, which has a 15 nm diameter core with six protruding arms (one 50 nm and the other five 35 nm in length, altogether 700,000 atoms). Periodic boundary conditions are applied along the lateral directions whereas a fixed boundary condition is applied along the vertical direction. In all simulations, the bottom-most 0.5 nm thick layer of the substrate atoms are spatially fixed to prevent vertical drift of the system. After the initial short energy minimization and equilibration of the components, simulations of the combined system are performed using the LAMMPS simulator³⁰ at the timestep of 0.001 ps under a canonical ensemble (NVT). Atomiclevel strain tensors of the substrate and WSe₂ monolayer due to the gold tips is calculated using the atomic strain modifier with the OVITO visualization software (see Supporting Information S1 for further details of the simulation method).³¹

Fig. 1e shows the simulated strain maps of the system. The deformation and strained regions are highly localized to a few nanometer areas that are in contact with the three AuNS tips and a maximum volumetric strain amplitude (local change in volumes before and after applying the strain) of around 6% can be obtained. This substantial strain field can cause modifications to the bandgap of the WSe₂ monolayers. We would like to mention that such highly localized strain profiles is beneficial for creating quantum emitters with high spatial precisions, provided that the

AuNS can be accurately placed at designated locations using nanopositioning techniques such as electrohydrodynamic printing, DNA-assisted self-assembly, and dip-pen nanolithography.²²⁻²⁴ More quantitative analysis of the strain profiles caused by the AuNS show that both compressive and tensile strains exist, with the former being stronger than the latter (see Supporting Information S2 for details). Although a maximum strain amplitude of around 6% is obtained, most of the atoms experience weaker strain fields with only 2.4% of them having strain fields larger than 1.0%.

Our spectroscopic studies of WSe₂ monolayers with AuNS deposited on top show strikingly different spectral features compared to those monolayers without AuNS. To perform the optical measurements, the samples were loaded into a continuous-flow liquid He cryostat on a home-built confocal laser microscope. A diode laser with a wavelength of 400 nm was used to excite the samples. WSe₂ monolayers used in this study were prepared by mechanical exfoliation of bulk materials. Fig. 2a and 2b show optical micrographs of representative WSe₂ monolayers. The as-

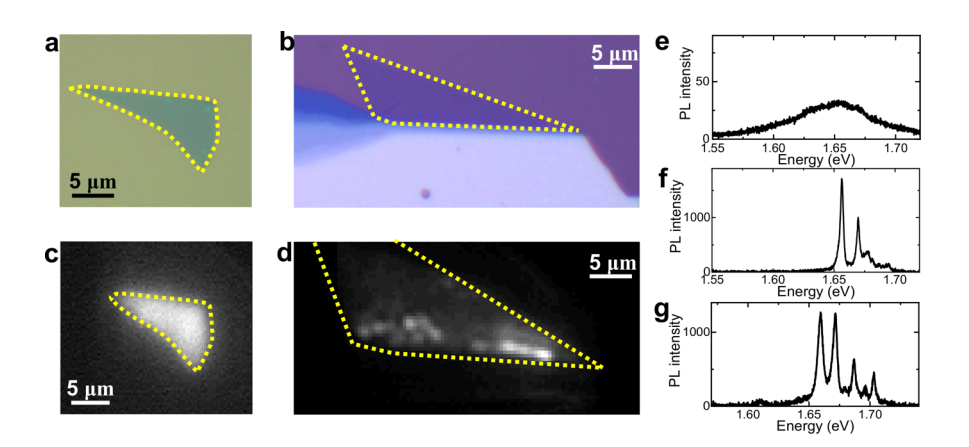


Figure 2. (a, c) Optical micrograph of a monolayer WSe₂ flake and the corresponding photoluminescence image. (b, d) Optical micrograph of a monolayer WSe₂ flake and the corresponding photoluminescence image with AuNS deposited on top. (e) Photoluminescence spectrum taken from the areas with relatively weak and homogeneous emission in (d). (f, g) Examples of photoluminescence spectra taken from the bright spots in (d).

exfoliated monolayers typically present homogeneous PL emission over the entire flake (see e.g. Fig. 2c). For those WSe₂ monolayers deposited with AuNS, spatial mapping of their PL intensities shows distinct localized bright spots superimposed on an apparently weaker and homogeneous PL background (Fig. 2d and Fig. S2). The PL spectra at the homogeneous background area show a rather broad peak centered at around 1.65 eV (Fig. 2e), characteristic of emission from excitons at defects sites in WSe₂ monolayers.³² The bright spots, in contrast, present sharp PL peaks superposed on the relatively broad defect emission peaks. Two such examples are shown in Fig. 2f and 2g, where distinct sharp peaks can be observed. Fig. 1c presents a histogram of the peak distributions constructed from such sharp PL spectral features.

To identify the quantum nature of the emitters giving rise to the sharp spectral features, we spectrally isolate the individual peak emission and perform second-order photon correlation spectroscopy measurements. Fig. 3a shows one such example, where an area ratio, defined as the ratio between the center peak area and the side peak average area, of 0.14 ± 0.03 is obtained, indicating the single photon nature of the corresponding quantum emitter. Of the 30 quantum emitters we studied, an average area ratio of 0.23 ± 0.021 can be derived (see Fig. 3b top for a histogram). We note that the non-zero area ratio is likely caused by imperfect blockage of backgrounds including residual emission from the defect sites and crosstalk between the two single photon detectors. This average area ratio value is very close to the value we obtained from quantum emitters created by dielectric nanopillars using a previously reported method^{18, 19} (0.23 \pm 0.032, Fig. 3b bottom). In this approach, dielectric nanopillars with a height of around 85 nm and a diameter of around 200 nm were fabricated by electron-beam lithography (see Supporting Information S1). When the WSe₂ monolayers are transferred onto the dielectric nanopillars, the 2D flakes conform to the contours of the nanopillars. The induced strains in the WSe₂ monolayers

can generate quantum defects (see Supporting Information S4 for exemplary data of the quantum emitters created by the dielectric nanopillars). Because of their relatively low refractive index, the dielectric nanopillars do not support apparent resonance modes at the relevant wavelengths. Therefore, they can create local strain fields in the WSe₂ monolayers without introducing extra influence from surface plasmons. We use these quantum emitters created by the dielectric nanopillars, which for clarity will be referred to as "uncoupled" quantum emitters, as references to study the influence of the AuNS surface plasmons. For the bright PL spots created by the AuNS, we obtain 3.4 ± 0.28 quantum emitters per site on average (Fig. 3e), close to the number of contact tips for each AuNS (Fig. 1e). These findings are consistent with our molecular dynamics simulations and suggest that the sharp tips of the AuNS can induce large enough local strains to enable the localization of excitons. Previous studies on local strain engineering have focused on WSe₂ monolayers mechanically draped over pillar structures or alike to create strain fields in the monolayers at the pillar top. 18-20 In an alternative approach, atomic force microscope tips have been successfully utilized to create indentation in WSe₂ monolayers on deformable substrates.³³ Due to the atomic thickness of the TMD monolayers, the creation of quantum emitters is extremely sensitive to the relative deformation of the TMD monolayers, with sharp pillars or tips only being able to create quantum defects with moderate spatial precision due to the potential risk of piercing the TMD layers. In our case, despite the extreme sharpness of the gold tips, the direct contact of the TMD monolayers with the underlying substrates avoids this issue and allows the creation of highly confined strain profiles.

A closer interrogation of the quantum emitter PL spectra further reveals their quantum nature. While stable PL spectra can be observed in some quantum emitters (Fig. 3c and the spectra at 1.67 eV in Fig. 3d), PL blinking and spectral diffusion can be observed in some other quantum emitters

(Fig. 3d, the bottom spectra at 1.65 eV), which are related to local field fluctuations caused by environmental perturbations.³⁴⁻³⁸ In rare occasions, such as in the specific case of the quantum emitter at ~ 1.65 eV shown in Fig. 3d, a spectral jump potentially correlated with the switching of the quantum emitter between its neutral exciton and multiexciton states (such as trions or biexcitons) can be observed. This kind of switching behavior has previously been observed in semiconductor quantum dots and quantum rings,³⁸⁻⁴² and can be controlled by the injection or extraction of charge carriers to the localized quantum emitters.⁴³ Our PL intensity dependent lifetime analysis of the quantum emitters (see Supporting Information S5 for details) shows that higher PL intensities are correlated with longer lifetimes, an effect that has previously been used

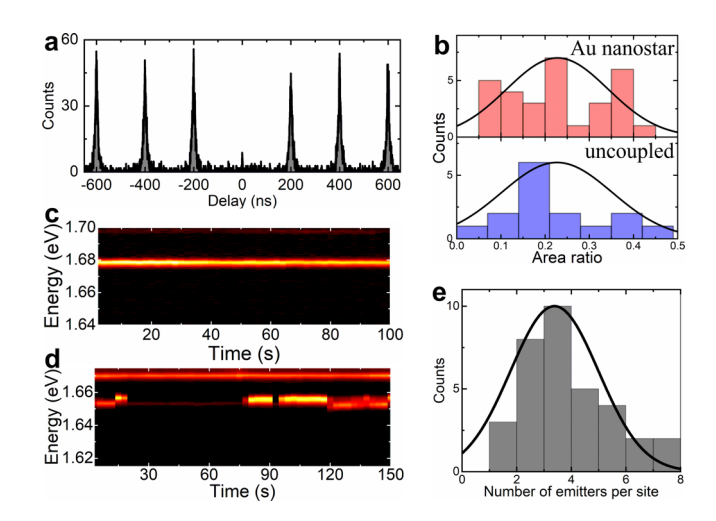


Figure 3. (a) A second-order photo-correlation trace of a quantum emitter. The corresponding PL peak is centered at $1.64~\rm eV$ and the collection range is selected to be around $8~\rm meV$. An area ratio of $0.14~\pm~0.03$ is observed. (b) Histograms of the area ratios of quantum emitters created by the Au nanostars (top) and the dielectric nanopillars (bottom). (c, d) Representative time-dependent photoluminescence spectra of quantum emitters created by Au nanostars. In (c), the photoluminescence spectra stay constant without spectral shift and blinking. In (d), a spectral jump between two states can be observed for one of the quantum emitters. (e) Histogram of the number of quantum emitters per site created by the Au nanostars.

to assign neutral exciton and multiexciton states.⁴⁴ This observation further supports our assumption of the occasional switching between the neutral and multiexciton states in the quantum emitters. We note that the PL blinking and spectral diffusion behavior can be observed in quantum emitters created by both AuNS and dielectric nanopillars. Likely, any carrier dynamics changes in the quantum emitters caused by coupling to the AuNS is not sufficient to suppress PL blinking and spectral diffusion, which has previously been observed in some quantum dot-surface plasmon systems.^{45, 46}

The influence of the surface plasmons on the emission properties of the nearby quantum emitters is further investigated by using the quantum emitters created by the dielectric nanopillars as the references. The effect of the surface plasmons is reflected in the PL decay dynamics of the quantum emitters. Fig. 4a shows representative PL decay curves collected from individual quantum emitters created by AuNS (red) and dielectric nanopillars (blue). Fitting the decay curves with singleexponential functions by deconvoluting the instrument response function gives rise to a PL lifetime of τ_{Au} = 4.5 ± 0.21 ns for the former and $\tau_{dielectric}$ = 11.2 ± 0.64 ns for the latter. This trend is held true in our measurements of 82 quantum emitters created by AuNS and 29 emitters by dielectric nanopillars, with the former yielding an average decay lifetime of 5.5 ± 0.66 ns, and the latter an average of 15.1 ± 1.67 ns (Fig. 4b). If we assume the lifetimes of the quantum emitters created by the dielectric nanopillars to be their uncoupled lifetimes, we obtain an average Purcell factor of $\tau_{\rm dielectric}/\tau_{\rm Au}=2.7$ for the AuNS. Previous studies have revealed that the Purcell factor of imperfect quantum emitters is typically larger than the measured decay rate enhancement.9 We expect a similar trend to exist in our system, that is, the exact Purcell factor of the AuNS-induced quantum emitters to be larger than 2.7 (see Supporting Information S6 for detailed discussions). Moreover, as can be seen from Fig. 1c, the coupling between the quantum emitter PL and the AuNS surface plasmons can be further optimized by overlapping the two peaks. This can be achieved by selective separation of AuNS⁴⁷ and utilizing those with maximum absorbance at around 1.65 eV. The coupling to the surface plasmons also leads to an increase in the PL intensity of the quantum emitters. On average, we observe a factor of 1.4 increase in the PL intensities of the quantum emitters created by AuNS compared to those created by the dielectric nanopillars (Fig. S5). We note here that the AuNS are covered by a self-assembled bilayer of buffer molecules (4-(2-hydroxyethyl)-1-piperazineethanesulfonic acid, HEPES), which is around 2 nm in total length in the aqueous solution.^{28, 48} This value gives an estimation of the distance between the Au nanotips and the underlying WSe₂ monolayers, although the real distance may vary due to reasons such as collapse of the bilayer molecules during the deposition process.

More interestingly, we observe two general categories of quantum emitters that show notably different PL behavior. In the coarsely defined first type of quantum emitters, those with high PL intensities are clearly associated with long emission wavelengths (Fig. 4c, green), whereas in the second type of quantum emitters, the emission wavelength-PL intensity dependence is almost obscure (Fig. 4c, orange) and the PL intensities of the quantum emitters are much weaker than the intensities of the first type. A similar effect is also observed in the quantum emitters created by the dielectric nanopillars (Fig. 4d), indicating that this effect is general and not related to the strain source. Local strain fields can modulate the bandgaps of TMD materials and induce spectral shifts in their PL emission. ^{49, 50} Moreover, recent theoretical calculations have predicted that the dark-bright excitonic energy separation in TMDs is dependent on local strains, with the two showing opposite strain-induced energy shifts. ⁵¹ Building on these understandings, we propose a possible mechanism that explains the very different PL behavior of the two groups of quantum emitters, as we explain below.

The lowest energy state in WSe₂ monolayers is an optically forbidden dark state that lies tens of meV below the lowest optically bright state.⁵² Our analysis of the second-order photon-correlation data of the quantum emitters in a timescale up to 15 µs shows a slight bunching superimposed on the antibunching signal (Supporting Information S8). This kind of long-term bunching in the photon correlation profile has been observed in other types of quantum emitters and is indicative of the existence of a dark trap state lying below the bright state.⁵³⁻⁵⁵ We believe that similar long-lived dark states also exist in our quantum emitters (Fig. 4e, left), consistent with previous studies predicting a lowest lying dark state⁵⁶ at around 10 meV below the lowest bright state.⁵⁷ At the experimental temperature used in our study, this means that majority of the photo-generated

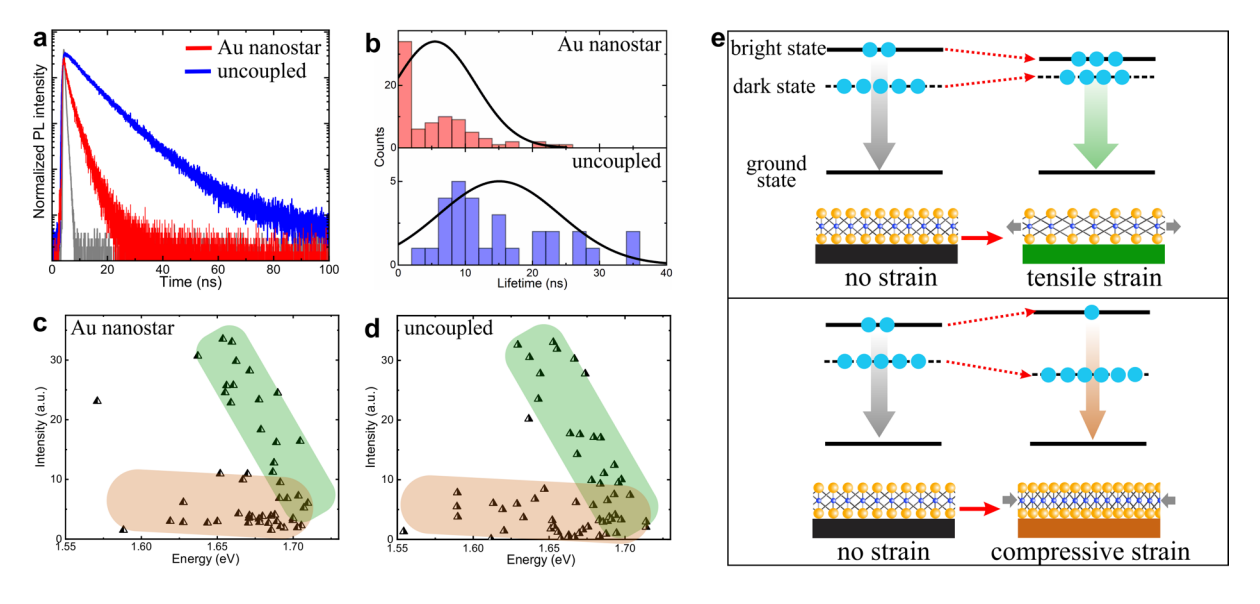


Figure 4. (a) Representative PL decay curves of individual quantum emitters created by Au nanostars (red) and dielectric nanopillars (blue). The corresponding instrument response function is also plotted (gray). (b) Histograms of the PL lifetimes of quantum emitters created by Au nanostars (top) and dielectric nanopillars (bottom). (c, d) Emission energy-dependent PL intensities of quantum emitters created by Au nanostars (c) and dielectric nanopillars (d). (e) Schematics of the corresponding electronic state shift and exciton population change when monolayer WSe₂ experiences tensile (top) and compressive (bottom) strains.

excitons would populate the low-lying dark state if we assume that the exciton population follows the Boltzmann distribution, i.e. $N \propto 1/[\exp\left(\frac{\Delta E}{k_B T}\right)]$, where ΔE is the dark-bright energy separation.⁵⁸ When a quantum emitter experiences a local tensile strain, its lowest dark state shifts up in energy and the bright state shifts down, leading to a reduced dark-bright separation (Fig. 4e, upper panel).⁵¹ This, as a result, leads to an increased population of excitons in the bright state and increased PL intensity accompanying a red-shift in the PL emission. On the contrary, when a quantum emitter is subjected to a compressive strain, the up-shift of the bright state and downshift of the dark state leads to a larger dark-bright separation, and hence reduced exciton populations in the bright state, reduced PL intensities, and blue-shifted PL emission (Fig. 4e, lower panel). In principle, both types of strains would lead to higher PL intensities at lower emission energies. However, due to the very low measurement temperature, small variations in the darkbright energy separation could have profound effects on the exciton population distributions, and the quantum emitters modulated by tensile strains are likely to be much brighter than those by compressive strains. Specifically, assume the tensile and compressive strains cause changes to the dark-bright energy splitting by ΔE_T and ΔE_C , respectively. The PL intensity ratio between a quantum emitter subject to the tensile and compressive strains can then be represented by $\eta =$ $e^{(\Delta E_T + \Delta E_C)/k_BT}$ (see Supporting Information S9 for details). This indicates that a quantum emitter would be brighter when it experiences tensile strains compared to when it experiences compressive strains. The clear distinction between the two groups of quantum emitters in Fig. 4c and 4d suggests the different natures of strains they experience. From the average PL intensity ratios between the two groups of quantum emitters, we obtain $\Delta E_T + \Delta E_C$ of around 0.55 meV and 0.57 meV for the AuNS- and nanopillar-induced quantum emitters, respectively. These values are in a good agreement with the strains we obtained from the molecular dynamics simulations and

previously reported strain values induced by the nanopillars.^{9, 18, 59} Accordingly, we assign the groups of quantum emitters with higher PL intensities (highlighted by green in Fig. 4c and 4d) to those modulated by tensile strains, and those with lower PL intensities (highlighted by orange in Fig. 4c and 4d) modulated by compressive strains.

In summary, we investigate the influence of AuNS on the emission properties of WSe₂ monolayers. By depositing AuNS on WSe₂ monolayers, localized bright spots with sharp emission peaks emerge. Photon-antibunching, which is a hallmark of single photon emission, can be observed from the sharp emission peaks, indicating their quantum nature. Our molecular dynamics simulations identify the origins of the quantum emitters to be the highly localized strain fields created by the tip ends of the AuNS. Moreover, due to the coupling of the quantum emitters to the surface plasmon modes in the AuNS, a reduction in the PL lifetime and an increase in the PL intensity can be observed for the quantum emitters. We also observe two types of PL intensity – emission energy correlation in the quantum emitters, which we attribute to the distinct strain fields they experience and the existence of a low-lying dark state in their electronic structures. Our study presents an alternative "bottom-up" approach for creating bright single-photon emitters in TMDs from colloidal systems. The findings from this study may also deepen our understanding of the electronic fine structures of the quantum defects and their precise control using external strain fields.

ASSOCIATED CONTENT

Supporting Information. This material is available free of charge via the internet at

http://pubs.acs.org.

Details of the experimental methods and molecular dynamics simulations; quantitative analysis of

the strain maps obtained from the molecular dynamics simulations; AuNS-induced quantum

emitters in WSe₂ monolayers; examples of quantum emitters created by dielectric nanopillars; PL

intensity-dependent lifetime analysis of the quantum emitters; numerical simulations of the PL

decay rate and quantum efficiency; histograms of PL intensities of quantum emitters created by

AuNS and dielectric nanopillars; second-order photon correlation spectroscopy of quantum

emitters; calculations of the strain-induced bright-dark splitting (PDF).

Corresponding Author

E-mail: xuedan.ma@anl.gov

Acknowledgements

This work was performed at the Center for Nanoscale Materials, a U.S. Department of Energy

Office of Science User Facility, and supported by the U.S. Department of Energy, Office of

Science, under Contract No. DE-AC02-06CH11357. T. W. O. and P. C. acknowledge supports

from the National Science Foundation under award no. CHE-1808502.

Competing interests

The authors declare no competing financial interests.

15

References

- 1. Chakraborty, C.; Kinnischtzke, L.; Goodfellow, K. M.; Beams, R.; Vamivakas, A. N. Voltage-controlled quantum light from an atomically thin semiconductor. *Nat. Nanotechnol.* **2015**, *10*, 507-511.
- 2. He, Y.-M.; Clark, G.; Schaibley, J. R.; He, Y.; Chen, M.-C.; Wei, Y.-J.; Ding, X.; Zhang, Q.; Yao, W.; Xu, X.; Lu, C.-Y.; Pan, J.-W. . Single quantum emitters in monolayer semiconductors. *Nat. Nanotechnol.* **2015**, *10*, 497-502.
- 3. Koperski, M.; Nogajewski, K.; Arora, A.; Cherkez, V.; Mallet, P.; Veuillen, J.-Y.; Marcus, J.; Kossacki, P.; Potemski, M. Single photon emitters in exfoliated WSe2 structures. *Nat. Nanotechnol.* **2015**, *10*, 503-506.
- 4. Srivastava, A.; Sidler, M.; Allain, A. V.; Lembke, D. S.; Kis, A.; Imamoğlu, A. Optically active quantum dots in monolayer WSe2. *Nat. Nanotechnol.* **2015**, *10*, 491-496.
- 5. Tonndorf, P.; Schmidt, R.; Schneider, R.; Kern, J.; Buscema, M.; Steele, G. A.; Castellanos-Gomez, A.; van der Zant, H. S. J.; de Vasconcellos, S. M.; Bratschitsch, R. Single-photon emission from localized excitons in an atomically thin semiconductor. *Optica* **2015**, *2*, 347-352.
- 6. Aharonovich, I.; Englund, D.; Toth, M. Solid-state single-photon emitters. *Nat. Photon.* **2016**, *10*, 631-641.
- 7. Toth, M.; Aharonovich, I. Single Photon Sources in Atomically Thin Materials. *Annu. Rev. Phys. Chem.* **2019**, *70*, 123-142.
- 8. Tripathi, L. N.; Iff, O.; Betzold, S.; Dusanowski, L.; Emmerling, M.; Moon, K.; Lee, Y. J.; Kwon, S.-H.; Höfling, S.; Schneider, C. Spontaneous Emission Enhancement in Strain-Induced WSe2 Monolayer-Based Quantum Light Sources on Metallic Surfaces. *ACS Photon.* **2018**, *5*, 1919-1926.
- 9. Luo, Y.; Shepard, G. D.; Ardelean, J. V.; Rhodes, D. A.; Kim, B.; Barmak, K.; Hone, J. C.; Strauf, S. Deterministic coupling of site-controlled quantum emitters in monolayer WSe2 to plasmonic nanocavities. *Nat. Nanotechnol.* **2018**, *13*, 1137-1142.
- 10. Cai, Y.; Kim, J.-H.; Yang, Z.; Dutta, S.; Aghaeimeibodi, S.; Waks, E. Radiative Enhancement of Single Quantum Emitters in WSe2 Monolayers Using Site-Controlled Metallic Nanopillars. *ACS Photon.* **2018**, *5*, 3466-3471.
- 11. Chakraborty, C.; Goodfellow, K. M.; Dhara, S.; Yoshimura, A.; Meunier, V.; Vamivakas, A. N. Quantum-confined Stark effect of individual defects in a van der Waals heterostructure. *Nano Lett.* **2017**, *17*, 2253-2258.
- 12. Iff, O.; Tedeschi, D.; Martín-Sánchez, J.; Moczała-Dusanowska, M.; Tongay, S.; Yumigeta, K.; Taboada-Gutiérrez, J.; Savaresi, M.; Rastelli, A.; Alonso-González, P.; Höfling, S.; Trotta, R.; Schneider, C. Strain-Tunable Single Photon Sources in WSe2 Monolayers. *Nano Lett.* **2019**, *19*, 6931-6936.

- 13. Liu, G.-B.; Pang, H.; Yao, Y.; Yao, W. Intervalley coupling by quantum dot confinement potentials in monolayer transition metal dichalcogenides. *New J. Phys.* **2014**, *16*, 105011.
- 14. Pawłowski, J.; Żebrowski, D.; Bednarek, S. Valley qubit in a gated MoS2 monolayer quantum dot. *Phys. Rev. B* **2018**, *97*, 155412.
- 15. Haldar, S.; Vovusha, H.; Yadav, M. K.; Eriksson, O.; Sanyal, B. Systematic Study of Structural, Electronic, and Optical Properties of Atomic-Scale Defects in the Two-Dimensional Transition Metal Dichalcogenides MX2 (M = Mo, W; X = S, Se, Te). *Phys. Rev. B* **2015**, *92*, 235408.
- 16. Zhang, S.; Wang, C.-G.; Li, M.-Y.; Huang, D.; Li, L.-J.; Ji, W.; Wu, S. Defect Structure of Localized Excitons in a WSe2 Monolayer. *Phys. Rev. Lett.* **2017**, *119*, 046101.
- 17. Zheng, Y. J.; Chen, Y.; Huang, Y. L.; Gogoi, P. K.; Li, M.-Y.; Li, L.-J.; Trevisanutto, P. E.; Wang, Q.; Pennycook, S. K.; Wee, A. T. S.; QUek, S. Y. Point Defects and Localized Excitons in 2D WSe2. *ACS Nano* **2019**, *13*, 6050-6059.
- 18. Branny, A.; Kumar, S.; Proux, R.; Gerardot, B. D. Deterministic strain-induced arrays of quantum emitters in a two-dimensional semiconductor. *Nat. Commun.* **2017**, *8*, 15053.
- 19. Palacios-Berraquero, C.; Kara, D. M.; Montblanch, A. R.-P.; Barbone, M.; Latawiec, P.; Yoon, D.; Ott, A. K.; Loncar, M.; Ferrari, A. C.; Atatüre, M. Large-scale quantum-emitter arrays in atomically thin semiconductors. *Nat. Commun.* **2017**, *8*, 15093.
- 20. Kern, J.; Niehues, I.; Tonndorf, P.; Schmidt, R.; Wigger, D.; Schneider, R.; Stiehm, T.; de Vasconcellos, S. M.; Reiter, D. E.; Kuhn, T.; Bratschitsch, R. Nanoscale Positioning of Single-Photon Emitters in Atomically Thin WSe2. *Adv. Mater.* **2016**, *28*, 7101-7105.
- 21. Klein, J.; Lorke, M.; Florian, M.; Sigger, F.; Sigl, L.; Rey, S.; Wierzbowski, J.; Cerne, J.; Müller, K.; Mitterreiter, E.; Zimmermann, P.; Taniguchi, T.; Watanabe, K.; Wurstbauer, U.; Kaniber, M.; Knap, M.; Schmidt, R.; Finley, J. J.; Holleitner, A. W. Site-selectively generated photon emitters in monolayer MoS2 via local helium ion irradiation. *Nat. Commun.* **2019**, *10*, 2755.
- 22. Gopinath, A.; Miyazono, E.; Faraon, A.; Rothemund, P. KW. K. Engineering and mapping nanocavity emission via precision placement of DNA origami. *Nature* **2016**, *535*, 401-405.
- 23. Hail, C. U.; Höller, C.; Matsuzaki, K.; Rohner, P.; Renger, J.; Sandoghdar, V.; Poulikakos, D.; Eghlidi, H. Nanoprinting organic molecules at the quantum level. *Nat. Commun.* **2019**, *10*, 1880.
- 24. Liao, X.; Brown, K. A.; Schumcker, A. L.; Liu, G.;He, S.; Shim, W.; Mirkin, C. A. Desktop nanofabrication with massively multiplexed beam pen lithography. *Nat. Commun.* **2013**, *4*, 2103.
- 25. Hail. C. U.; Höller, C.; Matsuzaki, K.; Rohner, P.; Renger, J.; Sandoghdar, V.; Poulikakos, D.; Eghlidi, H. . Nanoprinting organic molecules at the quantum level. *Nat. Commun.* **2019**, *10*, 3263.

- 26. Grzelczak, M., Pérez-Juste, J., Mulvaney, P., Liz-Marzán, L. M. Shape control in gold nanoparticle synthesis. *Chem. Soc. Rev.* **2008**, *37*, 1783-1791.
- 27. Li, N., Zhao, P., Astruc, D. Anisotropic Gold Nanoparticles: Synthesis, Properties, Applications, and Toxicity. *Angew. Chem. Int. Ed.* **2014**, *53*, 1756-1789.
- 28. Chandra, K.; Culver, K. S. B.; Werner, S. E.; Lee, R. C.; Odom, T. W. Manipulating the Anisotropic Structure of Gold Nanostars using Good's Buffers. *Chem. Mater.* **2016**, *28*, 6763-6769.
- 29. Hao, F.; Nehl, C. L.; Hafner, J. H.; Nordlander, P. Plasmon Resonances of a Gold Nanostar. *Nano Lett.* **2007**, *7*, 729-732.
- 30. Plimpton, S. Fast Parallel Algorithms for Short-Range Molecular Dynamics. *J. Comput. Phys.* **1995,** *117*, 1-19.
- 31. Stukowski, A. Visualization and analysis of atomistic simulation data with OVITO-the Open Visualization Tool. *Modelling Simul. Mater. Sci. Eng.* **2009**, *18*, 015012.
- 32. Tongay, S., Suh, J., Ataca, C., Fan, W., Luce, A., Kang, J. S., Liu, J., Ko, C., Raghunathanan, R., Zhou, J., Ogletree, F., Li, J., Grossman, J. C., Wu, J. Defects activated photoluminescence in two-dimensional semiconductors: interplay between bound, charged and free excitons. *Sci. Rep.* **2013**, *3*, 2657.
- 33. Rosenberger, M. R.; Dass, C. K.; Chuang, H.-J.; Sivaram, S. V.; McCreary, K. M.; Hendrickson, J. R.; Jonker, B. T. Quantum Calligraphy: Writing Single-Photon Emitters in a Two-Dimensional Materials Platform. *ACS Nano* **2019**, *13*, 904-912.
- 34. Efros, Al. L.; Nesbitt, D. J. Origin and Control of Blinking in Quantum Dots. *Nat. Nanotechnol.* **2016**, *11*, 661-671.
- 35. Ma, X.; Tan, H.; Kipp, T.; Mews, A. Fluorescence Enhancement, Blinking Suppression, and Gray States of Individual Semiconductor Nanocrystals Close to Gold Nanoparticles. *Nano Lett.* **2010**, *10*, 4166-4174.
- 36. Empedocles, S. A.; Bawendi, M. G. Quantum-Confined Stark Effect in Single CdSe Nanocrystallite Quantum Dots. *Science* **1997**, *278*, 2114-2117.
- 37. Ma, X.; Roslyak, O.; Wang, F.; Duque, J. G.; Piryatinski, A.; Doorn, S. K.; Htoon, H. Influence of Exciton Dimensionality on Spectral Diffusion of Single-Walled Carbon Nanotubes. *ACS Nano* **2014**, *8*, 10613-10620.
- 38. Hartmann, N.; Otten, M.; Fedin, I.; Talapin, D.; Cygorek, M.; Hawrylak, P.; Korkusinski, M.; Gray, S.; Hartschuh, A.; Ma, X. Uniaxial transition dipole moments in semiconductor quantum rings caused by broken rotational symmetry. *Nat. Commun.* **2019**, *10*, 3253.
- 39. Shimizu, K. T.; Woo, W. K.; Fisher, B. R.; Eisler, H. J.; Bawendi, M. G. Surface-Enhanced Emission from Single Semiconductor Nanocrystals. *Phys. Rev. Lett.* **2002**, *89*, 117401.

- 40. Warburton, R. J. . Single Spins in Self-Assembled Quantum Dots. *Nat. Mater.* **2013**, *12*, 483-493.
- 41. Warburton, R. J.; Schäflein, C.; Haft, D.; Bickel, F.; Lorke, A.; Karrai, K.; Garcia, J. M.; Schoenfeld, W.; Petroff, P. M. Optical emission from a charge-tunable quantum ring. *Nature* **2000**, *405*, 926-929.
- 42. Peng, L.; Otten, M.; Hazarika, A.; Coropceanu, I.; Cygorek, M.; Wiederrecht, G. P.; Hawrylak, P.; Talapin, D. V.; Ma, X. Bright trion emission from semiconductor nanoplatelets. *Phys. Rev. Mater.* **2020**, *4*, 056006.
- 43. Chakraborty, C.; Qiu, L.; Konthasinghe, K.; Mukherjee, A.; Dhara,S.; Vamivakas, N. 3D Localized Trions in Monolayer WSe2 in a Charge Tunable van der Waals Heterostructure. *Nano Lett.* **2018**, *18*, 2859-2863.
- 44. Park, Y.-S.; Bae, W. K.; Pietryga, J. M.; Klimov, V. I. Auger Recombination of Biexcitons and Negative and Positive Trions in Individual Quantum Dots. *ACS Nano* **2014**, *8*, 7288-7296.
- 45. Canneson, D., Mallek-Zouari, I., Buil, S., Quélin, X., Javaux, C., Mahler, B., Dubertret, B., Hermier, J.-P. Strong Purcell effect observed in single thick-shell CdSe/CdS nanocrystals coupled to localized surface plasmons. *Phys. Rev. B* **2011**, *84*, 245423.
- 46. Ma, X., Tan, H., Kipp, T., Mews, A. Fluorescence Enhancement, Blinking Suppression, and Gray States of Individual Semiconductor Nanocrystals Close to Gold Nanoparticles. *Nano Lett.* **2010**, *10*, 4166-4174.
- 47. Chandra, K.; Kumar, V.; Werner, S. E.; Odom, T. W. Separation of Stabilized MOPS Gold Nanostars by Density Gradient Centrifugation. *ACS Omega* **2017**, *2*, 4878-4884.
- 48. Liu, H.; Xu, Y.; Qin, Y.; Sanderson, W.; Crowley, D.; Turner, C. H.; Bao, Y. Ligand-Directed Formation of Gold Tetrapod Nanostructures. *J. Phys. Chem. C* **2013**, *117*, 17143-17150.
- 49. Castellanos-Gomez, A.; Roldán, R.; Cappelluti, E.; Buscema, M.; Guinea, F.; Van Der Zant, H. S. J.; Steele, G. A. Local Strain Engineering in Atomically Thin MoS2. *Nano Lett.* **2013**, *13*, 5361-5366.
- 50. Niehues, I.; Schmidt, R.; Drüppel, M.; Marauhn, P.; Christiansen, D.; Selig, M.; Berghäuser, G.; Wigger, D.; Schneider, R.; Braasch, L.; Koch, R.; Castellanos-Gomez, A.; Kuhn, T.; Knorr, A.; Malic, E.; Rohlfing, M.; Michaelis de Vasconcellos, S.; Bratschitsch, R. Strain Control of Exciton—Phonon Coupling in Atomically Thin Semiconductors. *Nano Lett.* **2018**, *18*, 1751-1757.
- 51. Feierabend, M.; Khatibi, Z.; Berghäuser, G.; Malic, E. Dark exciton based strain sensing in tungsten-based transition metal dichalcogenides. *Phys. Rev. B* **2019**, *99*, 195454.
- 52. Zhang, X.-X.; You, Y.; Zhao, S. Y. F.; Heinz, T. F. Experimental Evidence for Dark Excitons in Monolayer WSe₂. *Phys. Rev. Lett.* **2015**, *115*, 257403.

- 53. Gali, A.; Maze, J. R. Ab initio study of the split silicon-vacancy defect in diamond: Electronic structure and related properties. *Phys. Rev. B* **2013**, *88*, 235205.
- 54. Berthel, M.; Mollet, O.; Dantelle, G.; Gacoin, T.; Huant, S.; Drezet, A. Photophysics of single nitrogen-vacancy centers in diamond nanocrystals. *Phys. Rev. B* **2015**, *91*, 035308.
- 55. Ma, X.; Hartmann, N. F.; Baldwin, J. K. S.; Doorn, S. K.; Htoon, H. Room-temperature single-photon generation from solitary dopants of carbon nanotubes. *Nat. Nanotechnol.* **2015**, *10*, 671-675.
- 56. Dass, C. K.; Khan, M. A.; Clark, G.; Simon, J. A.; Gibson, R.; Mou, S.; Xu, X.; Leuenberger, M. N.; Hendrickson, J. R. Ultra-Long Lifetimes of Single Quantum Emitters in Monolayer WSe2/hBN Heterostructures. *Adv. Quantum Technol.* **2019**, *2*, 1900022.
- 57. He, Y.-M.; Höfling, S.; Schneider, C. Phonon induced line broadening and population of the dark exciton in a deeply trapped localized emitter in monolayer WSe₂. *Opt. Exp.* **2016**, *24*, 8066-8073.
- 58. Moskalenko, S. A.; Snoke, D. W. *Bose-Einstein Condensation of Excitons and Biexcitons*; Cambridge University Press: Cambridge, 2000.
- 59. Johari, P.; Shenoy, V. B. Tuning the Electronic Properties of Semiconducting Transition Metal Dichalcogenides by Applying Mechanical Strains. *ACS Nano* **2012**, *6*, 5449-5456.



